Check for updates

View Article Online
View Journal

Catalysis Science & Technology

Accepted Manuscript

This article can be cited before page numbers have been issued, to do this please use: D. Liu, J. Wang, Y. Wang and Y. Zhu, *Catal. Sci. Technol.*, 2018, DOI: 10.1039/C8CY00409A.

This is an Accepted Manuscript, which has been through the Royal Society of Chemistry peer review process and has been accepted for publication.

Accepted Manuscripts are published online shortly after acceptance, before technical editing, formatting and proof reading. Using this free service, authors can make their results available to the community, in citable form, before we publish the edited article. We will replace this Accepted Manuscript with the edited and formatted Advance Article as soon as it is available.

You can find more information about Accepted Manuscripts in the author guidelines.

Please note that technical editing may introduce minor changes to the text and/or graphics, which may alter content. The journal's standard Terms & Conditions and the ethical guidelines, outlined in our author and reviewer resource centre, still apply. In no event shall the Royal Society of Chemistry be held responsible for any errors or omissions in this Accepted Manuscript or any consequences arising from the use of any information it contains.

ROYAL SOCIETY OF CHEMISTRY

rsc.li/catalysis

View Article Online
DOI: 10.1039/C8CY00409A

Journal Name

ARTICLE

Anion exchange strategy for construction of a novel Bi_2SiO_5/Bi_2MoO_6 heterostructure with enhanced photocatalytic performance

Received 00th January 20xx,
Accepted 00th January 20xx

DOI: 10.1039/x0xx00000x

www.rsc.org/

Di Liu,[a] Jun Wang,[b] Yonggang Wang *[a] and Yongfa Zhu*[b]

Based on the structural similarity and the driving principle of solubility, we successfully constructed heterostructures of Bi_2SiO_5/Bi_2MoO_6 through an anion exchange strategy between the starting material of Bi_2MoO_6 and the incoming ions of SiO_3^{2-}. By tuning the adding amount of incoming SiO_3^{2-}, the evolution process of the Bi_2SiO_5/Bi_2MoO_6 heterostructures involving phase formation, morphology transformation, changes of specific surface area and optical properties were clearly identified. More importantly, the heterostructured products displayed remarkably enhanced photodegradation activities under UV and visible light irradiation than pure Bi_2MoO_6, which could be mainly ascribed to the relatively high surface areas, light-harvesting contribution from the Bi_2MoO_6 component, and effective separation of photo-generated electrons-holes driven by the interfacial potential difference upon the Bi_2SiO_5/Bi_2MoO_6 heterojunctions.

Introduction

Recently, Bi-based photocatalysts such as Bi_2O_3,[1] $CaBi_2O_4$,[2] Bi_2WO_6,[3] $BiVO_4$,[4] $BiPO_4$,[5] $Bi_2O_2CO_3$,[6] $Bi_4Ti_3O_{12}$,[7] Bi_2SiO_5 [8] and BiOX (X=Cl, Br, I) [9] have been reported to be effective photocatalysts due to their non-negligible merits such as unique electronic energy band structure, low toxicity, high stability and a wealth of element resources supplement. Bi-based oxy-acid salt catalysts (Bi_2WO_6, $BiVO_4$, Bi_2MoO_6 and Bi_2SiO_5) were generally considered to be the hybridization of Bi_2O_3 and corresponding oxides (WO_3, V_2O_5, Mo_2O_3 and SiO_2) with stoichiometric ratio. Thereby, these Bi-based oxy-acid salts exhibit similar structures consisting of alternately grown $[Bi_2O_2]^{2+}$ slabs and anion layers along c-axis direction, which belong to the Aurivillius family. Among them, Bi_2MoO_6 is reported as an excellent visible-light photocatalyst with a narrow band gap (2.5-2.8 eV), exhibits decent photocatalytic activity for O_2 evolution via water splitting [10] and degradation ability over organic pollutants.[11] However, due to its poor photocatalytic efficiency originating from the rapid recombination of photo-generated electrons and holes,[12] Bi_2MoO_6 still falls far from the requirements for practical application. As is known to us all, constructing of a heterojunction is an effective strategy to extend the spectral response range of semiconductor photocatalysts and simultaneously improve the photocatalytic activity by promoting the separation of photo-generated electrons and holes.[13] So far, many heterojunctions concerning Bi_2MoO_6 have been reported, such as TiO_2/ Bi_2MoO_6,[14] g-C_3N_4/Bi_2MoO_6,[15] $Bi_2O_2CO_3/Bi_2MoO_6$,[16] $BiOBr/Bi_2MoO_6$,[17] CdS/Bi_2MoO_6,[18] $BiOCl/Bi_2MoO_6$,[19] $Ag/AgCl/Bi_2MoO_6$,[20] BiOI/Bi2MoO6,[21] $BiIO_4/Bi_2MoO_6$,[22] Bi_2S_3/Bi_2MoO_6[23] and $Bi_{3.64}Mo_{0.36}O_{6.55}/Bi_2MoO_6$,[24] these Bi_2MoO_6-based heterojunctions showed increased photocatalytic efficiency in comparison with bare Bi_2MoO_6 photocatalyst. Inspired by this, we also dedicated to the construction of novel Bi_2MoO_6-based heterojunction to further advance its photocatalytic activity. As two Aurivillius structured photocatalysts, Bi_2MoO_6 and Bi_2SiO_5 are both crystallized in layered structures consisting of $[Bi_2O_2]^{2+}$ file layers interleaved with anion slabs.[25] At a result, compared to Bi_2MoO_6, similar structure and a lower solubility of Bi_2SiO_5 makes it thermodynamically favored for Bi_2MoO_6 transformed into Bi_2SiO_5 via the anion exchange reaction, and consequently the Bi_2SiO_5/Bi_2MoO_6 heterojunction can be obtained. To the best of our knowledge, no previous studies regarding Bi_2SiO_5/Bi_2MoO_6 heterostructure have been reported.

Herein, as expected, we successfully synthesized the novel Bi_2SiO_5/Bi_2MoO_6 heterostructures through the anion exchange reaction between the starting precursor of Bi_2MoO_6 solid microspheres and incoming ions of SiO_3^{2-} under a one-pot hydrothermal treatment. Experimental results successfully demonstrate the formation of Bi_2SiO_5/Bi_2MoO_6 heterostructures which meantime show greatly improved photocatalytic activities towards the photo-degradation of pollutants (phenol and methyl orange) under visible light and UV irradiation. Through analysis of their electronic energy

[a] School of Chemical & Environmental Engineering, China University of Mining and Technology, Beijing 100083, P. R. China.
[b] Department of Chemistry, Tsinghua University, Beijing 100084, P. R. China.
E-mail: wangyg@cumtb.edu.cn

Electronic Supplementary Information (ESI) available: [EDX, HRTEM, photocatalytic degradation curves on MO, BET, time-resolved PL decay curves and ESR spectra data.]. See DOI: 10.1039/x0xx00000x

Published on 24 May 2018. Downloaded by Hacettepe Universitesi on 27/05/2018 07:18:18.

Catalysis Science & Technology Accepted Manuscript

View Article Online
DOI: 10.1039/C8CY00409A

Published on 24 May 2018. Downloaded by Hacettepe Universitesi on 27/05/2018 07:18:18.

band structures, surface areas and transient PL decay spectra, it was concluded that the excellent photocatalytic activity could be ascribed to the extended light harvest from the component of Bi_2MoO_6, relatively higher specific surface area and the improved migration efficiency of photo-induced carriers upon the interfaces of Bi_2SiO_5 and Bi_2MoO_6.

Experimental

Materials preparation

For the synthesis of starting precursor of Bi_2MoO_6, 5 mmol $Bi(NO_3)_3{\cdot}5H_2O$ and 2.5 mmol $Na_2MoO_4{\cdot}2H_2O$ was dissolved together in a 250 mL flask with 120 mL distilled water under stirring, and the pH of the mixed suspension was adjusted to about 6 using a NaOH solution (2 M). Then, the resulting suspension was refluxed under 100℃ for 20 h. After the reactions finished, the flask was cooled to room temperature, and the as-prepared precipitates were collected via centrifugation, washed with deionized water and ethanol for several times, and subsequently dried at 80℃ for 10 h. For the synthesis of the heterostructured samples, Na_2SiO_3 (0, 0.2 mmol, 0.5 mmol, 1 mmol, 2 mmol) was dissolved respectively with 80 mL distilled water, and each 0.5 g Bi_2MoO_6 precursor was added to the above solutions under vigorous stirring. After well stirred for 30 min, the resulting suspensions were transferred into Teflon-lined autoclaves of 100 mL capacity and treated at 160℃ for 16 h. When the reactions was finished, the autoclaves were cooled to the room temperature naturally. Eventually, the as-prepared precipitates were collected via centrifugation, washed with deionized water and ethanol for several times, and subsequently dried at 80℃ for 10 h. The as-prepared samples with different adding amount of Na_2SiO_3 ranging from 0 to 2 mmol were labeled as Bi_2MoO_6, S-0.2, S-0.5, S-1 and S-2, respectively.

Sythesis of the control sample of pure Bi_2SiO_5 [26]: 6 mmol $Bi(NO_3)_3{\cdot}5H_2O$ and 3 mmol $Na_2SiO_3{\cdot}9H_2O$ was dissolved into 40 mL ethylene glycol and 40 mL deionized water under vigorous stirring, respectively. The $Na_2SiO_3{\cdot}9H_2O$ solution was then added to the solution of $Bi(NO_3)_3{\cdot}5H_2O$, a white suspension formed immediately. Finally, the pH of the mixed suspension was adjusted to 12 using a NaOH solution (2 M). After stirred for 30 min, the mixture was transferred into a 100 mL capacity Teflon-lined autoclave and hydrothermally treated at 200 ℃ for 10 h. Then, the autoclave was cooled to room temperature naturally. The precipitates were collected by centrifugation, and washed with deionized water and ethanol for several times, and finally dried in oven at 80 ℃ for 10 h.

Characterizations

A Rigaku D/max-2400 X-ray diffractometer using a Cu Kα1 (λ = 0.15418 nm) at 40kV and 200 mA was adopted to collect X-ray diffraction (XRD) patterns of the as-prepared samples. Fourier transform infrared spectra (FT-IR) were obtained using a Bruker VERTEX 700 spectrometer in the frequency range of 1800-600 cm^{-1} with a resolution of 4 cm^{-1}. The morphologies and sizes of the as-prepared samples and their energy dispersive spectrometer (EDS) analysis were carried out using a SU-8010 field emission Scanning Electron Microscope (SEM). High-resolution transmission electron microscopy (HRTEM) images were collected at a JEOL JEM-2010F field emission transmission electron microscope with an accelerating voltage of 200 kV. The Brunauer–Emmett–Teller (BET) surface area measurements were performed using a Micromeritics (ASAP 2010V5.02H) surface area analyzer. The nitrogen adsorption and desorption isotherms were measured at 77 K after degassing the samples on a Sorptomatic 1900 Carlo Erba Instrument. UV–vis spectra and UV-vis diffuse reflectance spectra (DRS) were obtained on a Hitachi U-3010 UV-vis spectrophotometer. The total organic carbon (TOC) analyzer (Multi N/C 2100, Analytik Jena AG) was applied to analyse the mineralization degree of targeted pollutant of phenol. Electron spin resonance (ESR) spectra were recorded from the sample mixture, containing spin-trapping probes such as 5,5-dimethyl-1-pirroline-N-oxide (DMPO) and samples, after exposure to visible light and UV light for selected times using an Endor spectrometer (JEOL ES-ED3X) at room temperature. The time-resolved PL decay spectra were collected at a Fluorescence Spectrometer (Edinburgh Instruments, FLS920).

Photocatalytic experiments

Photo-degradation on two targeted pollutants of phenol and methyl orange (MO) under visible and UV light irradiation was carried out to evaluate the photocatalytic activity of the as-prepared samples. Before the light irradiation, a suspension of a 50 mL probe pollutants solution and 30 mg photocatalysts was stirred for 0.5 h under dark to reach the adsorption-desorption equilibrium. The visible light source was acquired by a 500 W xenon lamp equipped with a cut-off filter (⩾ 420 nm) and the UV light was acquired by a 300 W mercury lamp equipped with bandpass filter (365±10 nm). At given time intervals, a suspension (2 mL) was extracted and centrifuged to remove the photocatalysts. The concentrations of probe pollutants were characterized by a HPLC system (Shimadzu LC-20AT) with a C18 reversed phase column and a Hitachi U-3010 UV–vis spectrophotometer.

Results and discussion

Formation of Heterostructures

Fig.1 shows the XRD patterns of the as-prepared samples fabricated by hydrothermal procedure at different adding amount of SiO_3^{2-} (0-2 mmol). The JCPDS card of Bi_2MoO_6 and Bi_2SiO_5 are listed for comparisons. It can be seen from Fig. 1 that when there is no adding of SiO_3^{2-} during the hydrothermal reaction, that is sample Bi_2MoO_6, all of its diffraction peaks can be clearly indexed to orthorhombic phase of Bi_2MoO_6 (JCPDS No. 84-0787). As the adding amount of SiO_3^{2-} increased to 0.2~1 mmol, the as-prepared samples showed the coexistence of Bi_2MoO_6 (JCPDS No. 84-0787) and Bi_2SiO_5 (JCPDS No. 75-1483) through identification of the area labeled by an orange dotted rectangle in Fig. 1. When the adding amount of SiO_3^{2-} was increased to 2 mmol, the product mainly shows pure Bi_2SiO_5 phase. As a result, the above XRD results of S-0.2~S-2

Catalysis Science & Technology Accepted Manuscript

This journal is © The Royal Society of Chemistry 20xx

View Article Online
DOI: 10.1039/C8CY00409A

Published on 24 May 2018. Downloaded by Hacettepe Universitesi on 27/05/2018 07:18:18.

demonstrate that the sacrificial material of Bi_2MoO_6 partly or fully transformed into Bi_2SiO_5 via an anion exchange reaction, thus successfully constructing of Bi_2SiO_5/Bi_2MoO_6 heterostructures (S-0.2~S-1).

Successful formation of heterostructures and the evolution process of the products with increasing adding amount of SiO_3^{2-} can also be revealed by FT-IR and Raman spectrum as shown in Fig. 2. For Bi_2MoO_6, absorption bands in the range of 910-650 cm^{-1} are mainly referred to Mo-O stretching vibrations and deformation vibrations.[27] As previously reported,[28] the bands located at 842 and 796 cm^{-1} can be attributed to the asymmetric and symmetric stretching vibration mode of the corner sharing $(MoO_6)^{6-}$. The peak around 720 cm^{-1} can be assigned as the asymmetric stretching mode of MoO_6 involving vibrations of the equatorial oxygen atoms. Then, from observation of the top area of Fig. 2a, the peaks located around 856 cm^{-1}, 945 cm^{-1} and 1029 cm^{-1} are respectively related to the vibration modes of the Bi-O-Si bonds, the isolated $(SiO_5)^{6-}$ groups and the Si-O bond.[29] Therefore, FT-IR results confirmed the formation of Bi-O-Si and Si-O bonds in the as-prepared samples upon adding of SiO_3^{2-}, further proving the co-existence of Bi_2SiO_5 and Bi_2MoO_6 in sample S-0.2~S-1. Fig. 2b shows the Raman spectra evolution of the as-prepared samples obtained at different adding amount of SiO_3^{2-}. All the typical vibrational bands for Bi_2MoO_6 [28] can be observed from the black curve of sample Bi_2MoO_6. For sample S-0.2~S-1, similar Raman vibration modes but with different intensity in the range of 100-900 cm^{-1} can be found. The intensities of Bi_2MoO_6 characteristic vibrations decreased gradually with increasing addition of SiO_3^{2-}, indicating a growing transformation degree of Bi_2MoO_6. Moreover, when the adding amount of SiO_3^{2-} is high enough to 2 mmol, the characteristic vibrations of Bi_2MoO_6 disappeared, implying that the starting material of Bi_2MoO_6 would experience nearly full transformation into the Bi_2SiO_5 phase through SiO_3^{2-} substituting MoO_4^{2-}.

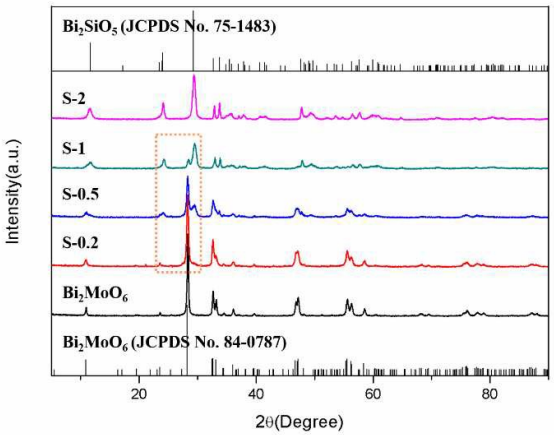

Fig. 1 XRD patterns of the as-prepared samples.

The morphology, size and component analysis of the as-prepared samples were characterized by SEM and EDX elemental mapping. As shown in Fig. 3, it can be seen that the starting material of Bi_2MoO_6 displays the morphology of irregularly hierarchical microspheres assembled by lots of tiny nanosheets. When SiO_3^{2-} was introduced into the hydrothermal reaction system, the morphology of S-0.2 did not show obvious difference in comparison with sample Bi_2MoO_6. However, further increasing the incoming amount of SiO_3^{2-}, embryonic polyhedron for S-0.5 and obvious polyhedron for S-1 appeared, as shown in Fig. 3c,d. Moreover, when the adding amount of SiO_3^{2-} reaches up to 2 mmol, that is sample S-2, widespread polyhedron with uniform distribution dominates the morphology. Obviously, the morphology transformation of the as-prepared samples originates from the addition of SiO_3^{2-} and the subsequent anion exchange during the hydrothermal reactions. This interesting morphology evolution inspire us to further investigate whether the distinct morphology of tiny nanoplate and polyhedron mass are attributed to two phases of Bi_2MoO_6 and Bi_2SiO_5, respectively. Fig. S1 and Fig. 3f exhibited the EDX elemental mapping results of two heterostructured samples of S-0.2 and S-1. Firstly, the EDX analysis further demonstrated that the Bi, Mo, Si, O elements coexisted in S-0.2 and S-1. Secondly, as the common element in Bi_2MoO_6 and Bi_2SiO_5, Bi was found homogeneously dispersed on the entire composite. It can be seen that, Mo, which comes from Bi_2MoO_6, was also distributed on the entire region of the composite. While as the own element of Bi_2SiO_5, Si was found to be uniformly dispersed along the shape of polyhedron through comparison with the corresponding SEM image shown in the insertion of Fig. 3f. Therefore, the results of EDX mapping verified our inference: the tiny nanoplate and polyhedron mass are assigned to two phases of Bi_2MoO_6 and Bi_2SiO_5, respectively.

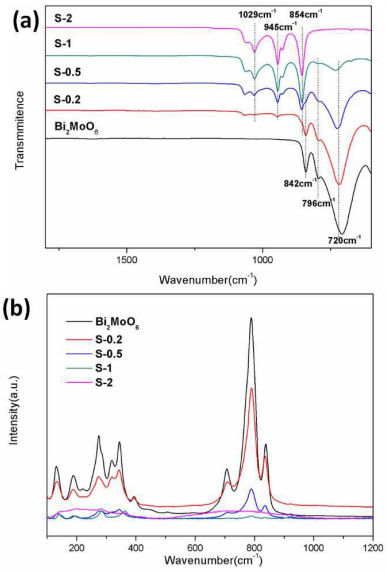

Fig. 2 FT-IR (a) and Raman (b) spectra of the as-prepared samples.

Catalysis Science & Technology Accepted Manuscript

View Article Online
DOI: 10.1039/C8CY00409A

Typical HRTEM images shown in Fig. S2 further depict the detailed Bi_2SiO_5/Bi_2MoO_6 nanojunction structure for sample S-0.2 and S-1. The measured interplanar spacings are about 0.326 and 0.379 nm shown in Fig. S2a, which correspond well to the (140) planes of orthorhombic Bi_2MoO_6 and the (400) planes of orthorhombic Bi_2SiO_5, respectively. Fringes spaced by 0.379 and 0.191 nm, and by 0.274 nm in Fig. S2b correspond to the (400) and (022) crystal planes of Bi_2SiO_5, and (200) crystal planes of Bi_2MoO_6, respectively. High lattice match between the two components would not only help successful growth of heterostructures,[30] but also make the heterostructures remain stable during the photocatalytic reaction.[31] Here, the d-spacing of (140) planes of Bi_2MoO_6 (0.326 nm) is quite close to the d-spacing (0.379 nm) at the Bi_2SiO_5 (400) facet, revealing clear compatibility in lattices upon the interfaces of the two phases of Bi_2SiO_5 and Bi_2MoO_6. It is reasonable to deduce that close matching of lattice between two materials could greatly facilitate the interfacial charge transfer.

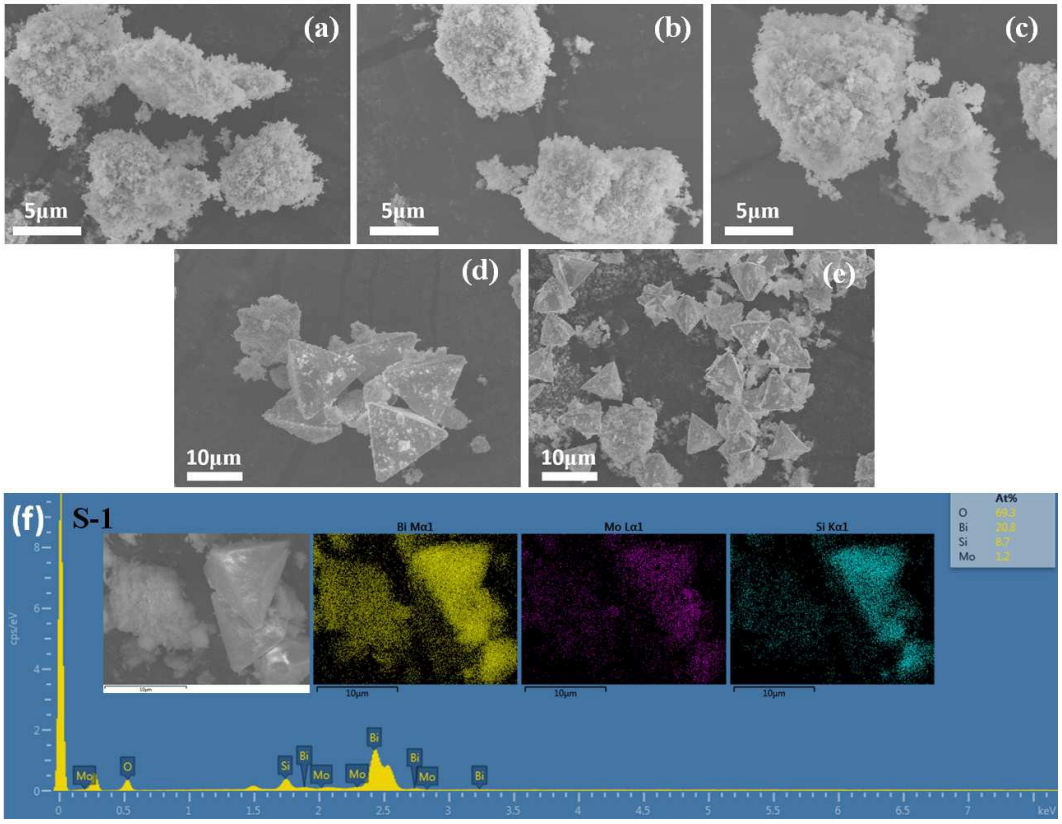

Fig. 3 SEM images of sample Bi_2MoO_6 (a), S-0.2 (b), S-0.5 (c), S-1 (d) and S-2 (e); EDX analysis of sample S-1 and the corresponding SEM image and elemental mapping of Bi, Mo, Si (f).

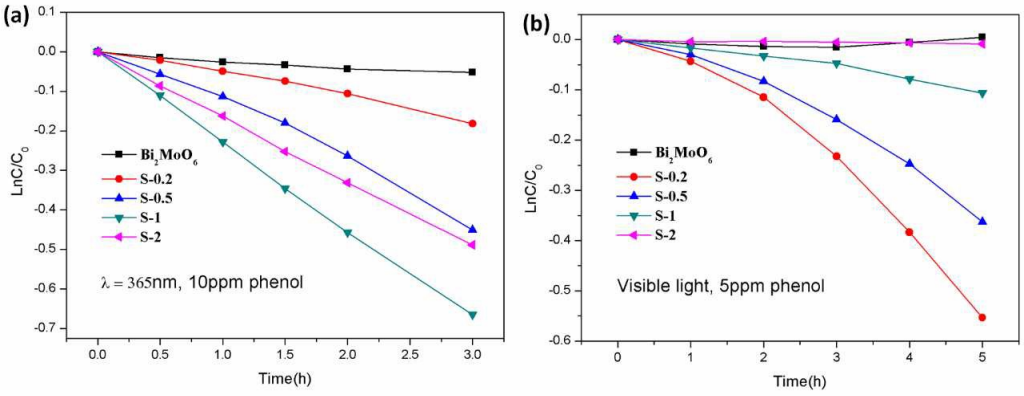

Fig. 4 Photocatalytic degradation efficiencies on phenol by the as-prepared samples under UV-light ($\lambda \approx 365$ nm) (a) and visible light ($\lambda \geqslant 420$ nm) (b) irradiation.

Published on 24 May 2018. Downloaded by Hacettepe Universitesi on 27/05/2018 07:18:18.
Catalysis Science & Technology Accepted Manuscript

This journal is © The Royal Society of Chemistry 20xx

View Article Online
DOI: 10.1039/C8CY00409A

Published on 24 May 2018. Downloaded by Hacettepe Universitesi on 27/05/2018 07:18:18.

Catalysis Science & Technology Accepted Manuscript

Photocatalytic Performance

The photocatalytic performances of the as-prepared samples with different adding amount of SiO_3^{2-} were studied by photodegradation of colorless phenol or MO under visible light and UV light irradiation, respectively, as shown in Fig. 4 and Fig. S3. As the adding amount of SiO_3^{2-} increases, the photocatalytic activities for degradation over phenol and MO under UV light irradiation of the as-prepared samples increase first, achieve a peak value at sample S-1, and then decrease. And the visible light photocatalytic activities of the as-prepared samples also show a trend of ascending firstly and then descended with the increasing of SiO_3^{2-} except for the difference that sample S-0.2 exhibits the best visible light activity. Through identifying the intermediate products of the photocatalytic degradation over phenol based on their retention times from HPLC chromatographys,[32] as shown in Fig. S4, the intermediate products of phenol oxidation in this photocatalytic reaction for sample S-0.2 and S-1 can be both attributed to hydroquinol, p-benzoquinone/catechol and bi-phenol. The removal of TOC was also conducted to reveal the mineralization degree over phenol. It can be seen from Fig. S5 that, for S-1, with prolonging time under 365 nm light irradiation, the removal percent of TOC continuously increased and reached up to ca. 25% after 3 h. For sample S-0.2, the removal percent of TOC was achieved to ca. 23% after visible light irradiation of 5h. The results of TOC removal efficiencies for S-1 and S-0.2 were both less than their degradation efficiencies over phenol which was 48.6% for S-1 and 42.5% for S-0.2 under the same irradiation time (see Fig. 4), suggesting that the photo-oxidation paths over phenol contains both the process of transformation into some intermediate products and subsequent mineralization process.

In order to find out the stabilities of sample S-0.2 and S-1, the cyclic degradation experiments were further conducted. The catalyst recovered from the first (1st) cycle is reused as it is subjected for the second (2nd) cycle and the same is continued up to 4 cycles. Due to inevitable loss of catalyst in the process of recycling, it is reasonable that the photo-degradation efficiency would decrease some after four cyclic tests. Herein, from observation of Fig. S6, the results of four continuous cyclic photo-degradation over phenol indicated good stabilities of the photocatalytic performance for both S-0.2 and S-1.

Specifically, the photocatalytic mechanisms under visible light and UV light irradiations were systematically investigated, as detailed in the following part.

Photocatalytic Mechanism

BET specific surface area and pore volume of the as-prepared samples were analyzed through nitrogen adsorption–desorption isotherm and pore-size distribution curves. The isotherms of as-prepared samples can all be attributed to type IV with hysteresis loops close to type H3. Combined with their corresponding SEM pictures which show hierarchical architectures assembled by nanoplates, hysteresis loops of type H3 revealed the existence of slit-like pores formed by the accumulation of nanoplate-like particles. Importantly, as shown in Fig. S7, the BET surface area values and pore volume values of the as-prepared samples showed the trend of first increase and then decrease, among which sample S-0.5 exhibited the highest BET surface area value and the highest pore volume (Fig. S7c). As verified by the SEM analysis, with increasing adding amount of SiO_3^{2-}, the hierarchical architectures assembled by Bi_2MoO_6 nanoplates gradually evolved into Bi_2SiO_5 polyhedron structures through the ion exchange reaction. As a result, phase evolution from Bi_2MoO_6 into Bi_2SiO_5 and their corresponding morphology evolution from nanoplates into polyhedron structures resulted in hierarchical frameworks with roughness for sample S-0.2 and S-0.5 with relatively high BET surface area value and pore volume, whereas gradually decreased nanoplates and stacking slit-like pores for sample S-1 and S-2 may account for their lowered BET surface area values and pore volumes. It is noteworthy that the relatively higher BET surface area of sample S-0.2 and S-1 than sample Bi_2MoO_6 would provide more active sites for the photocatalytic reaction.

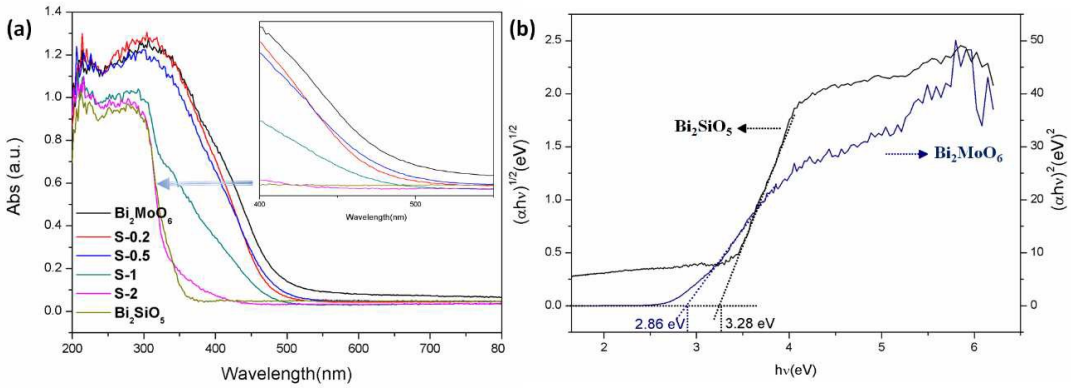

Fig. 5 UV-Vis diffuse reflection spectra (DRS) of the as-prepared samples (a); the plot of $(ahυ)^{1/2}$ or $(ahυ)^2$ vs. hυ of pure Bi_2SiO_5 and pure Bi_2MoO_6 (b).

View Article Online
DOI: 10.1039/C8CY00409A

Journal Name

ARTICLE

Published on 24 May 2018. Downloaded by Hacettepe Universitesi on 27/05/2018 07:18:18.

Catalysis Science & Technology Accepted Manuscript

UV-Vis diffuse reflection spectra (DRS) was adopted to investigate the optical absorption properties of the as-prepared samples. As shown in Fig. 5, the absorption edges exhibited gradual blue-shifts upon increasing adding of SiO_3^{2-}, indicating the rising constituent content of Bi_2SiO_5. Kubelka–Munk function of $\alpha h\upsilon = A(h\upsilon\text{-}E_g)^{n/2}$ was used to determine the band gap of the Bi_2SiO_5/Bi_2MoO_6 heterostructures, in which α, h, υ, E_g and A are absorption coefficient, Planck constant, light frequency, band-gap energy and a constant, respectively.[33] In this formula, the n value is set as 1 for direct transition and 4 for indirect transition. Herein, n values of Bi_2SiO_5 [34] and Bi_2MoO_6 [22] were 4 and 1, respectively. Through calculation from the tangent to the curves of $(ahv)^{2/n}$ versus (hv) shown in Fig. 5b, Eg of pure Bi_2SiO_5 and pure Bi_2MoO_6 were determined as 3.28 eV and 2.86 eV, respectively. The band edge positions of them can be estimated by empirical formulas of $E_{VB} = X - E^e + 0.5E_g$ [35] and $E_{CB} = E_{VB} - E_g$, where E_{VB}/E_{CB} is the valence band (VB)/conduction band (CB) edge potential, X represents the electronegativity of the semiconductor, E_g is the band-gap energy of the semiconductor, E^e is the energy of free electrons (4.5 eV). As previously reported, X values for Bi_2SiO_5 and Bi_2MoO_6 were determined as 6.474 eV [26] and 5.55 eV,[18] respectively. Accordingly, as depicted in Scheme 1, the E_{CB} and E_{VB} of pure Bi_2SiO_5 can be estimated to be +0.334 eV and +3.614 eV (vs. NHE), and that of pure Bi_2MoO_6 were -0.38 eV and +2.48 eV (vs. NHE). The results were very close to the previous reports revealing their electronic energy band positions.[36] As depicted above, Bi_2SiO_5 and Bi_2MoO_6 exhibited matched straddling band-structures, leading to the successful formation of a type-II heterojunction. When illuminated under UV light (365 nm), Bi_2SiO_5 and Bi_2MoO_6 both can absorb the photons, and the difference of band-potential between the two units of heterojunction would drive the opposite migration of photo-generated electrons and holes. Therefore, the spatial separation and accordingly long-lived photo-generated electrons and holes could be achieved. Showing the best visible light photocatalytic activity, in sample S-0.2, only Bi_2MoO_6 can be stimulated by the visible light, Bi_2SiO_5 would then serve as an electron acceptor, efficient spatial charge separation via the heterojunction interface still can be realized. Schematic illustrations of the band-gap structures and possible flow of charge carriers upon the heterostructured interfaces for S-1 under UV light illumination and S-0.2 under visible light illumination were shown in Scheme 1. Such higher efficiency of charge separation of the heterojunction thus would greatly enhance their photocatalytic performance. Moreover, time-resolved PL decay spectra and estimated emission lifetimes of the as-prepared samples were adopted to investigate the separation ability of photo-generated electron-hole pairs in the heterostructured samples.[37] As can be seen from Fig. S8, three decay curves are all well fitted by bi-exponential kinetic decay models, and all the emission lifetimes of the heterostructured samples of S-0.2 and S-1 are longer than that of Bi_2MoO_6. The prolonged lifetimes for sample S-0.2 and S-1 means effectively reduced recombination rate of the photo-generated electron-hole pairs, and thus improved charge separation abilities and photocatalytic activities.

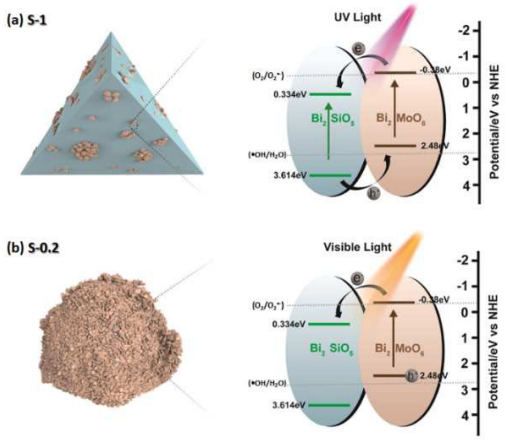

Scheme 1 Schematic illustration of the band-gap structure and possible flow of charge carriers in the Bi_2SiO_5/Bi_2MoO_6 heterostructured systems under UV light ($\lambda \approx 365$ nm) or visible light ($\lambda \geqslant 420$ nm) irradiation.

In order to further understand the mechanism of the photocatalytic process, in situ photocatalytic active species were detected through the ESR (electron paramagnetic resonance) technique.[32] Fig. S9 shows that no signals of DMPO-•OH adducts and DMPO-$O_2^{\bullet-}$ adducts appeared after visible light illumination for sample S-0.2. However, strong characteristic peaks of the DMPO-•OH adducts were observed for sample S-1 after 2 mins of UV light illumination, whereas $O_2^{\bullet-}$ radical was still not detected after 2 mins of UV light illumination. As can be seen from the illustration shown in Scheme 1b, for S-0.2, upon visible light irradiation, photo-generated electrons which would transfer to the CB of Bi_2SiO_5, could not produce $O_2^{\bullet-}$ through photo-reduction of dissolved O_2 because the CB potential of Bi_2SiO_5 was less negative than that of $O_2/O_2^{\bullet-}$ (-0.33 eV vs. NHE),[17] and the oxidizing ability of photo-generated holes left at the VB of Bi_2MoO_6 was also not enough to yield •OH radicals due to its shallower potential than that of $\bullet OH/H_2O$ (2.8 eV vs. NHE).[38] On this occasion, the

View Article Online
DOI: 10.1039/C8CY00409A

Published on 24 May 2018. Downloaded by Hacettepe Universitesi on 27/05/2018 07:18:18.

pollutants could mainly be photo-decomposed by direct holes which were spatial separated from photo-generated electrons and accordingly be long-lived at the VB of Bi_2MoO_6. Then, upon the interfaces of the heterojunction of S-1 shown in Scheme 1a, no yield of •OH and $O_2^{\bullet-}$ should be expected due to the limited oxidization and reduction capability of VB potential of Bi_2MoO_6 and CB potential of Bi_2SiO_5. Interestingly, strong signals of DMPO-•OH adducts for S-1 after 2 mins of UV light illumination appeared, this may be originated from the individually bare surfaces of Bi_2SiO_5 polyhedron which can give rise to •OH through its more positive potential than the redox potential of $•OH/H_2O$. As a result, in sample S-1, the pollutants could be easily photo-degraded by reactive species of •OH or holes.

Based on the above characterization results, on one side, with increasing adding amount of SiO_3^{2-}, growing transformation degree from Bi_2MoO_6 into Bi_2SiO_5 (that is continuously reduced ratio of Bi_2MoO_6:Bi_2SiO_5) was confirmed. On the other side, with the increasing of SiO_3^{2-}, the hierarchical architectures assembled by Bi_2MoO_6 tiny nanoplates gradually evolved into big Bi_2SiO_5 polyhedron structures through the ion exchange reaction, resulting in a trend of ascending firstly and then descended for the BET surface areas of the as-prepared samples. As a result, main component in S-0.2 and S-1 can be respectively identified as Bi_2MoO_6 and Bi_2SiO_5. Herein, moderate BET surface areas, hierarchical frameworks with roughness together with the aid of promoted separation efficiencies of photo-generated carriers upon the interfaces of Bi_2SiO_5/Bi_2MoO6, it was reasonable that S-0.2 showed the best visible light activity and S-1 exhibited the highest UV light activity.

Conclusions

In summary, to develop photocatalysts with high-efficiency for environmental purification, we constructed novel Bi_2SiO_5/Bi_2MoO_6 heterojunctions via an ion exchange strategy under hydrothermal process by using Bi_2MoO_6 as a sacrificial material. In addition, the heterostructured product with optimal UV/visible light catalytic activity could be achieved by adjusting the adding amount of incoming SiO_3^{2-}, which also greatly surpass the photocatalytic activities of pure Bi_2MoO_6 over degradation of phenol and MO. Their photocatalytic activity enhancements could be attributed to their relatively higher surface areas, the contribution of the enhanced light absorption of the Bi_2MoO_6 component and efficient charge carriers transfer driven by the interfacial potential difference of Bi_2SiO_5/Bi_2MoO_6, which was verified by their matched straddling energy band and PL decay spectra. This novel and powerful Bi_2SiO_5/Bi_2MoO_6 heterostructured system would have great potential in the area of water environmental purification.

Conflicts of interest

There are no conflicts to declare.

Acknowledgements

This work was financially supported by China Postdoctoral Science Foundation (No. 2017M620073).

Notes and references

1 L. Zhou, W. Wang, H. Xu, S. Sun, M. Shang, *Chem. - Eur. J.,* 2009, **15**, 1776-1782.
2 J. Tang, Z. Zou, J. Ye, *Angew. Chem., Int. Ed,* 2004, **43**, 4463-4466.
3 (a) C. Zhang, Y. Zhu, *Chem. Mater.,* 2005, **17**, 3537-3545; (b) F. Amano, A. Yamakata, K. Nogami, M. Osawa, B. Ohtani, *J. Am. Chem. Soc.,* 2008, **130**, 17650-17651; (c) L.-W. Zhang, Y.-J. Wang, H.-Y. Cheng, W.-Q. Yao, Y.-F. Zhu, *Adv. Mater.,* 2009, **21**, 1286-1290.
4 (a) A. Kudo, K. Omori, H. Kato, *J. Am. Chem. Soc.,* 1999, **121**, 11459-11467; (b) R. Li, F. Zhang, D. Wang, J. Yang, M. Li, J. Zhu, X. Zhou, H. Han, C. Li, *Nat. Commun.,* 2013, **4**, 1432.
5 (a) C. Pan, Y. Zhu, Environ. Sci. Technol., 2010, **44**, 5570-5574; (b) F. Tian, H. Zhao, G. Li, Z. Dai, Y. Liu, R. Chen, *ChemSusChem*, 2016, **9**, 1579-1585
6 H. Cheng, B. Huang, K. Yang, Z. Wang, X. Qin, X. Zhang, Y. Dai, *ChemPhysChem,* 2010, **11**, 2167-2173.
7 W. Wei, Y. Dai, B. Huang, *J. Phys. Chem. C,* 2009, **113**, 5658-5663.
8 R. Chen, J. Bi, L. Wu, W. Wang, Z. Li, X. Fu, *Inorg. Chem.,* 2009, **48**, 9072-9076.
9 X. Zhang, Z. Ai, F. Jia, L. Zhang, *J. Phys. Chem. C,* 2008, **112**, 747-753.
10 Y. Shimodaira, H. Kato, H. Kobayashi, A. Kudo, *J. Phys. Chem. B,* 2006, **110**, 17790-17797.
11 (a) X. Zhao, J. Qu, H. Liu, C. Hu, *Environ. Sci. Technol.,* 2007, **41**, 6802-6807; (b) G. Tian, Y. Chen, W. Zhou, K. Pan, Y. Dong, C. Tian, H. Fu, *J. Mater. Chem.,* 2011, **21**, 887-892; (c) Z. Dai, F. Qin, H. Zhao, J. Ding, Y. Liu, R. Chen, *ACS Catalysis*, 2016, **6**, 3180–3192.
12 W. Yin, W. Wang, S. Sun, *Catal. Commun.,* 2010, **11**, 647-650.
13 (a) H. Cheng, B. Huang, P. Wang, Z. Wang, Z. Lou, J. Wang, X. Qin, X. Zhang, Y. Dai, *Chem. Commun.,* 2011, **47**, 7054-7056; (b) A. Hameed, T. Montini, V. Gombac, P. Fornasiero, *J. Am. Chem. Soc.,*2008, 130, 9658-9659.
14 (a) J. Tian, P. Hao, N. Wei, H. Cui, H. Liu, *ACS Catal.,* 2015, **5**, 4530-4536; (b) M. Zhang, C. Shao, J. Mu, Z. Zhang, Z. Guo, P. Zhang, Y. Liu, *CrystEngComm*, 2012, **14**, 605-612.
15 (a) H. Li, J. Liu, W. Hou, N. Du, R. Zhang, X. Tao, *Appl. Catal., B,* 2014, **160-161**, 89-97; (b) T. Yan, Q. Yan, X. Wang, H. Liu, M. Li, S. Lu, W. Xu, M. Sun, *Dalton Trans.,* 2015, **44**, 1601-1611.
16 Y.-S. Xu, W.-D. Zhang, *Appl. Catal., B,* 2013, **140-141**, 306-316.
17 S. Wang, X. Yang, X. Zhang, X. Ding, Z. Yang, K. Dai, H. Chen, *Appl. Surf. Sci.,* 2017, **391**, 194-201.
18 Y. Feng, X. Yan, C. Liu, Y. Hong, L. Zhu, M. Zhou, W. Shi, *Appl. Surf. Sci.,* 2015, **353**, 87-94.
19 D. Yue, D. Chen, Z. Wang, H. Ding, R. Zong, Y. Zhu, *Phys. Chem. Chem. Phys.,* 2014, **16**, 26314-26321.
20 Q. Yan, M. Sun, T. Yan, M. Li, L. Yan, D. Wei, B. Du, *RSC Adv.,* 2015, **5**, 17245-17252.
21 T. Yan, M. Sun, H. Liu, T. Wu, X. Liu, Q. Yan, W. Xu, B. Du, *J. Alloys Compd.,* 2015, **634**, 223-231.
22 H. Huang, L. Liu, Y. Zhang, N. Tian, *J. Alloys Compd.,* 2015, **619**, 807-811.
23 J. Zhang, L. Zhang, N. Yu, K. Xu, S. Li, H. Wang, J. Liu, *RSC Adv.,* 2015, **5**, 75081-75088.

Catalysis Science & Technology Accepted Manuscript

View Article Online
DOI: 10.1039/C8CY00409A

24 Z. Dai, F. Qin, H. Zhao, F. Tian, Y. Liu, R. Chen, *Nanoscale*, 2015, **7**, 11991-11999.
25 (a) A. Ayame, K. Uchida, M. Iwataya, M. Miyamoto, *Appl. Catal., A,* 2002, **227**, 7-17; (b) D. Liu, W. Yao, J. Wang, Y. Liu, M. Zhang, Y. Zhu, *Appl. Catal., B,* 2015, **172-173**, 100-107.
26 X. Liu, W. Wang, Y. Liu, B. Huang, Y. Dai, X. Qin, X. Zhang, *RSC Adv.,* 2015, **5**, 55957-55963.
27 F. Trifirò, H. Hoser, R. D. Scarle, *J. Catal.,* 1972, **25**, 12-24.
28 L. Zhang, T. Xu, X. Zhao, Y. Zhu, *Appl. Catal., B,* 2010, **98**, 138-146.
29 D. Liu, J. Wang, M. Zhang, Y. Liu, Y. Zhu, *Nanoscale,* 2014, **6**, 15222-15227.
30 N. S. Pesika, Z. Hu, K. J. Stebe, P. C. Searson, *J. Phys. Chem. B,* 2002, **106**, 6985-6990.
31 C. Pan, J. Xu, Y. Wang, D. Li, Y. Zhu, *Adv. Funct. Mater.,* 2012, **22**, 1518-1524.
32 D. Liu, J. Wang, X. Bai, R. Zong, Y. Zhu, *Adv. Mater.*, 2016, **28**, 7284-7290.
33 S. Sun, W. Wang, L. Zhang, L. Zhou, W. Yin, M. Shang, *Environ. Sci. Technol.,* 2009, **43**, 2005-2010.
34 C.-C. Chen, C.-T. Yang, W.-H. Chung, J.-L. Chang, W.-Y. Lin, *J. Taiwan Inst. Chem. Eng.,* 2017, **78**, 157-167.
35 Y. F. Zhu, D. H. Fan, W. Z. Shen, *Langmuir,* 2008, **24**, 11131-11136.
36 (a) Z. Wan, G. Zhang, *J. Mater. Chem. A*, 2015, **3**, 16737-16745; (b) M. Zhang, C. Shao, J. Mu, X. Huang, Z. Zhang, Z. Guo, P. Zhang, Y. Liu, *J. Mater. Chem.,* 2012, **22**, 577-584.
37 Q. Zhang, Z. Dai, G. Cheng, Y. Liu, R. Chen, *Ceram. Int.*, 2017, **43**, 11296-11304.
38 S. Kumar, A. Baruah, S. Tonda, B. Kumar, V. Shanker, B. Sreedhar, *Nanoscale,* 2014, **6**, 4830-4842.

Published on 24 May 2018. Downloaded by Hacettepe Universitesi on 27/05/2018 07:18:18.

Catalysis Science & Technology Accepted Manuscript

This journal is © The Royal Society of Chemistry 20xx

View Article Online
DOI: 10.1039/C8CY00409A

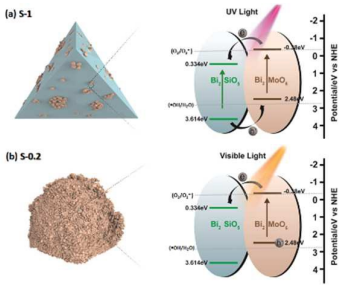

A novel Bi_2SiO_5/Bi_2MoO_6 heterojunction with highly efficient photocatalytic performance was successfully designed and constructed via an anion exchange strategy.

Published on 24 May 2018. Downloaded by Hacettepe Universitesi on 27/05/2018 07:18:18.

Catalysis Science & Technology Accepted Manuscript